Electronic Supporting Information (ESI)

Synergistic effects of extrinsic photoconduction and photogating in short-wavelength ZrS_3 infrared photodetector

Yiye Yu, [a,b] Meng Peng, [a] Fang Zhong,*[c] Zhen Wang, [b] Xun Ge, [b] Hao Chen, [b] Jiaxiang Guo, [b] Yang Wang, [d] Yue Chen, [b] Tengfei Xu, [d] Tiange Zhao, [b,e] Ting He, [c] Kun Zhang, [b] Feng Wu,*[a] Changqing Chen,*[a] Jiangnan Dai, [a] and Weida Hu [b,c,f]

a. Wuhan National Laboratory for Optoelectronics, Huazhong University of Science and Technology, Wuhan 430074, China.

b. State Key Laboratory of Infrared Physics, Shanghai Institute of Technical Physics, Chinese Academy of Sciences, Shanghai 200083, China.

c. Hangzhou Institute for Advanced Study, University of Chinese Academy of Sciences, Hangzhou 310024, China.

d. Fudan University, Shanghai 200433, China.

e. Sun Yat-Sen University, Guangzhou 510275, China.

f. University of Chinese Academy of Sciences, Beijing 100049, China.

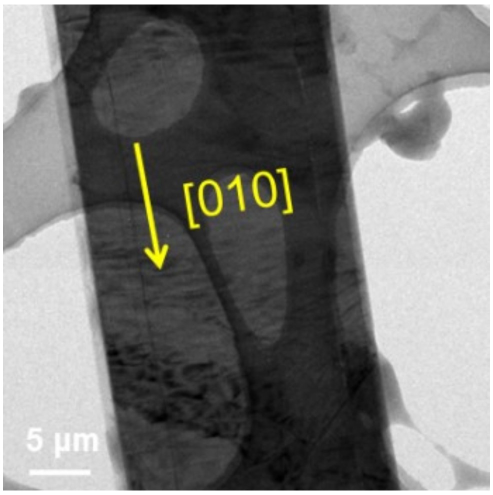

Fig. S1. Low-resolution TEM of ZrS_3 nanoflake along the [010] direction.

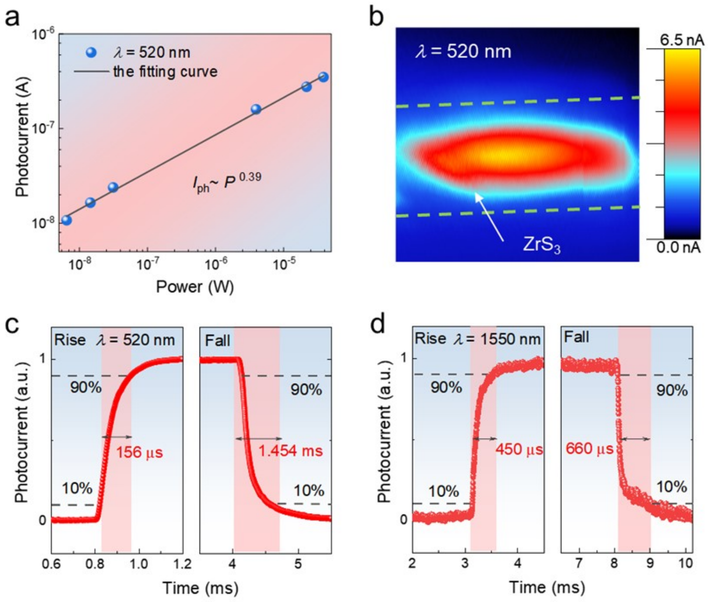

Fig. S2. Photoelectric properties of ZrS_3 photodetector. (a) Power-dependent photocurrent under 830 nm light illumination. The red line is a fitting curve following a power law. (b) Photocurrent mapping of ZrS_3 photodetector under 520 nm irradiation. The concentrated current site is located in the center of the channel, indicating that light is absorbed by ZrS_3 and electron-hole pairs are generated. (c) Response time of ZrS_3 photodetector under 520 nm illumination. Rising time and falling time are approximately 156 μs and 1.454 ms, respectively. The long falling time may be due to the long time taking for the carriers trapped by the defect to be fully released. (d) Response time of ZrS_3 photodetector under 1550 nm light irradiation. Rising time and falling time are approximately 450 μs and 660 μs, respectively. (Rising time and falling time are defined as the time from 10% to 90% and 90% to 10% at the maximum current value, respectively.)

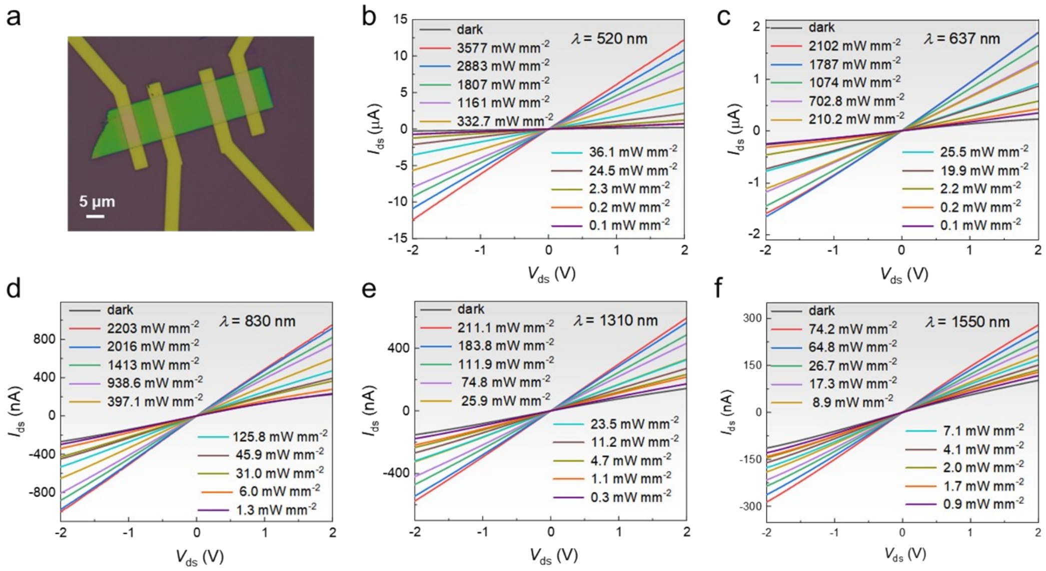

Fig. S3. *I-V* curves of ZrS_3 photodetector at the dark condition and different wavelength light illumination: (a) Optical microscopy image of ZrS_3 photodetector. (b-f) *I-V* curves of ZrS_3 photodetector at the dark condition and 520 nm, 637 nm, 830 nm, 1310 nm, and 1550 nm light illumination with different power densities.

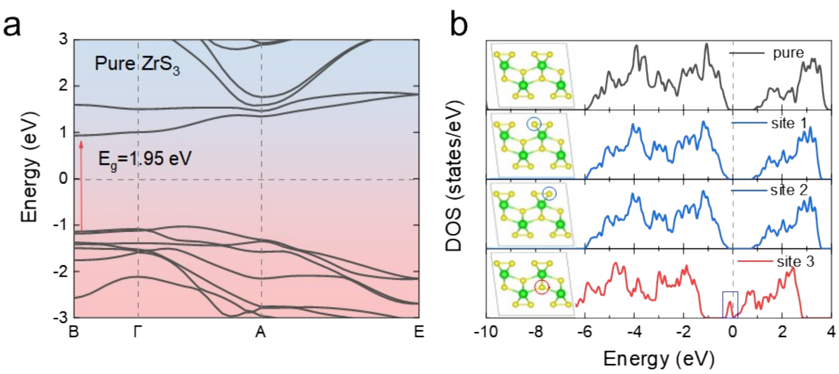

Fig. S4. (a) Energy band structure of pure ZrS_3. (b) The density of states (DOS) of pure ZrS_3 and ZrS_3 with S vacancies at different positions. Obviously, defect level is introduced into ZrS_3 bandgap when S vacancies appear at site 3, which represents sulfide (S^{2-}) vacancies.

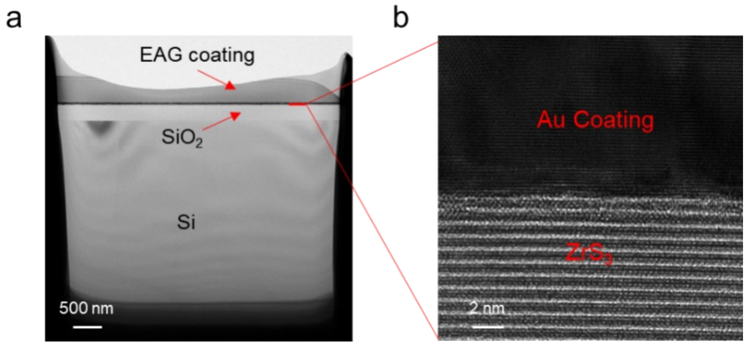

Fig. S5. Cross-sectional TEM of ZrS_3 with 20 nm gold (Au) coating. (a) Bright-field cross-sectional TEM of the ZrS_3 sample cut by the focused ion beam. (b) High-resolution TEM of the interface of ZrS_3 and 20 nm Au coating.

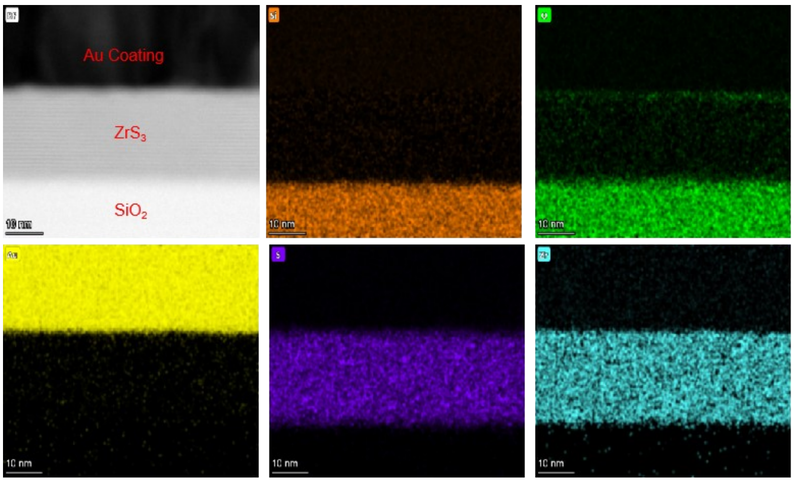

Fig. S6. EDS mapping of ZrS_3 with Au coating. The distribution of elements shows that there is no significant oxygen element enrichment in ZrS_3.

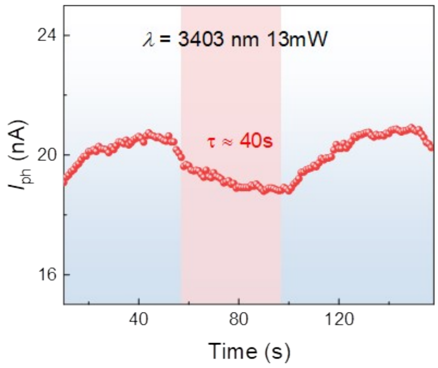

Fig. S7. Response of ZrS_3 photodetector under 3403 nm illumination. There is no obvious photocurrent in the mid-infrared band and a slow response time of about 40 seconds.

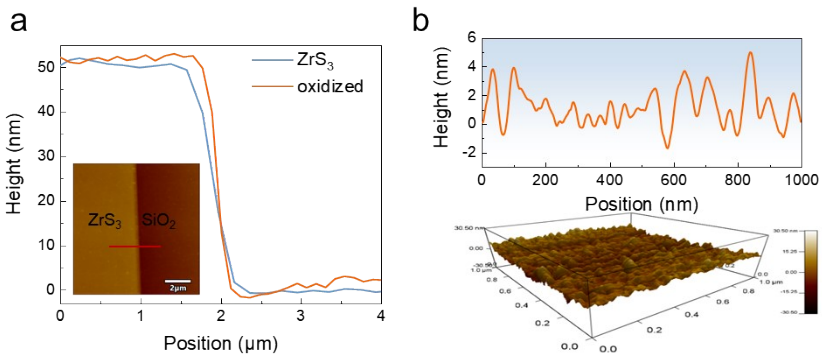

Fig. S8. Atomical force microscopy (AFM) characterization of ZrS_3 before and after oxidation (a) Thickness profiles of pure ZrS_3 nanobelts before and after the oxidization for two days in an atmospheric environment. The surface of the oxidized ZrS_3 becomes rough. The insert is the AFM image. (b) Surface roughness characterization of the oxidized ZrS_3. The top profile indicates that the surface of oxidized ZrS_3 with an average diameter of about 50nm irregularly; 3D height distribution map on the surface is shown on the bottom.

Note 1. The detection parameters of ZrS_3 photodetector.

In this work, three parameters of responsivity (*R*), external quantum efficiency (*EQE*), and detectivity (D^*) are used to evaluate the response performance of the ZrS_3 photodetector. These parameters are defined by equations as follows

$$R = \frac{I_{ph}}{A \times P}$$

where I_{ph} is the photocurrent, *A* is the active area, and *P* is the optical power density.

$$EQE = \frac{I_{ph}/e}{P/hv} = \frac{R \times 1240}{\lambda} \times 100\%$$

where *e* is the electron charge, *hv* is the photon energy, and λ (nm) is the wavelength of the laser.

$$D^* = \frac{R\sqrt{A\Delta f}}{i_n}$$

Where *R* is responsivity, *A* is the area of the channel, Δf is electrical bandwidth, i_n is the noise current.

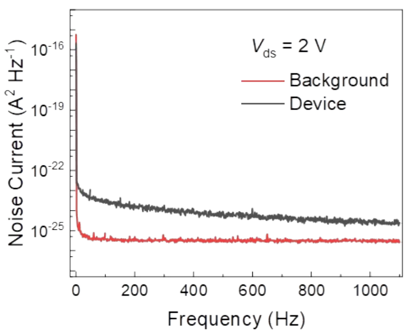

Fig. S9. Current noise spectral density under frequency from 1 Hz to 1100 Hz.

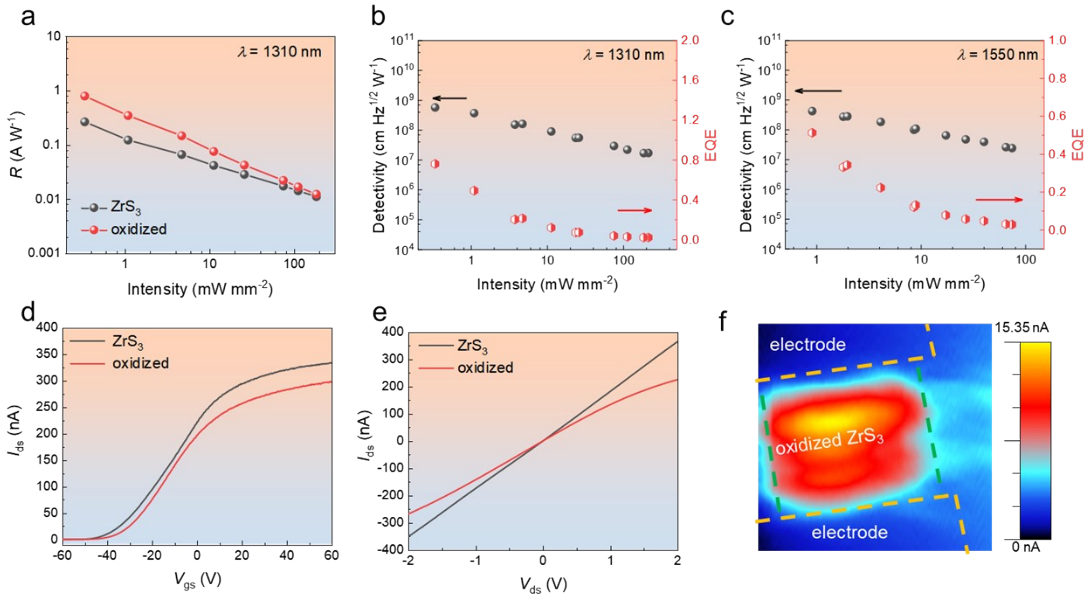

Fig. S10. Electrical and photoelectric properties of ZrS_3 photodetector with an oxide layer. (a) Responsivity (*R*) as a function of optical power density of ZrS_3 photodetector before and after oxidization under 1310 nm irradiation. (b-c) Detectivity (D^*) and external quantum efficiency (*EQE*) as a function of optical power density of ZrS_3 before and after oxidization under 1310 nm and 1550 nm irradiation. (d-e) The transfer and output curve of ZrS_3 before and after oxidization for two days. (f) The photocurrent mapping of oxidized ZrS_3 photodetector under 1550 nm laser illumination.

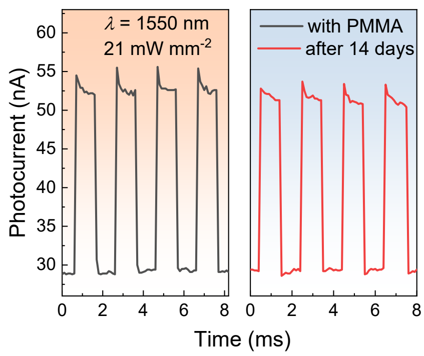

Fig. S11. Stability of ZrS_3 with an oxide layer. I-T curves of the ZrS_3 photodetector with an oxide layer were coated with PMMA again and placed in an atmospheric environment for 14 days. The oxidized ZrS_3 can still maintain a relatively stable response of 1550 nm light after 14 days under the protection of PMMA.

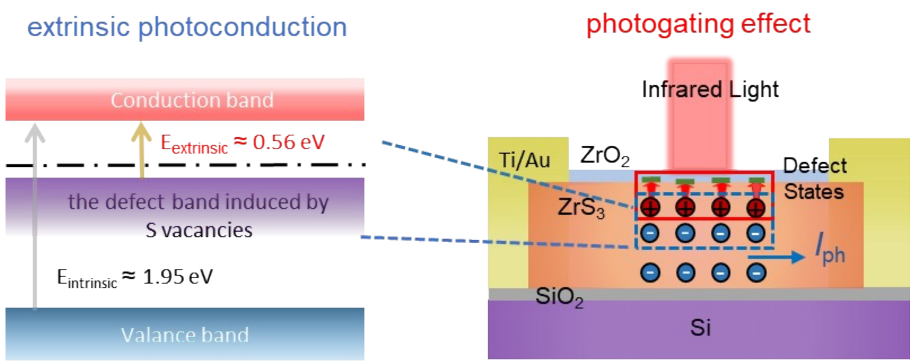

Fig. S12. The schematic diagram of the ZrS_3 photodetector with the synergistic effects of extrinsic photoconduction and photogating.

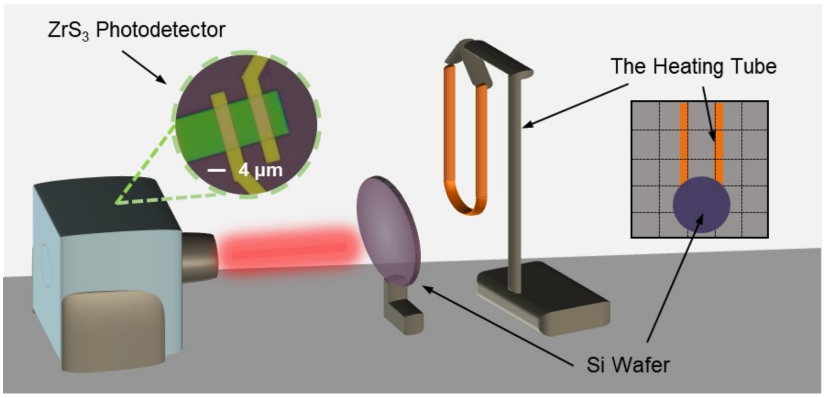

Fig. S13. The Schematic diagram of infrared imaging based on ZrS_3 photodetector.

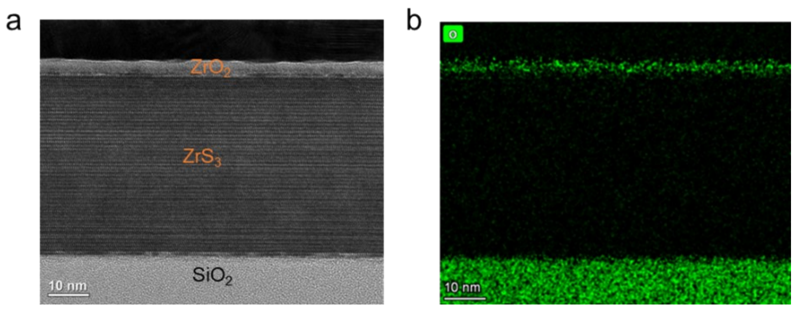

Fig. S14. a) The cross-sectional TEM image of oxidized ZrS_3, showing an oxide layer clearly; b) The oxygen EDS mapping of oxidized ZrS_3, showing oxygen element only exists on ZrO_2 and SiO_2.

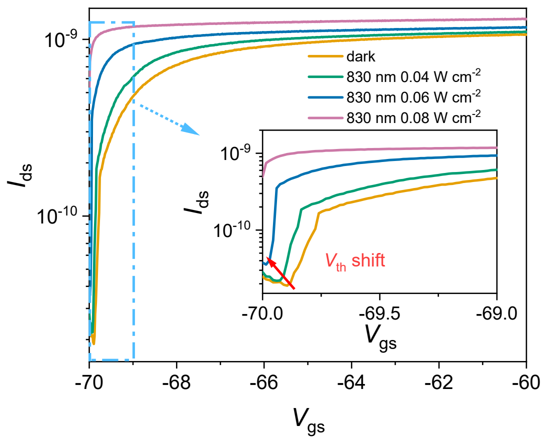

Fig. S15. The transfer characteristic curve of oxidized ZrS_3 photodetector under the dark condition and 830 nm infrared light illumination, V_{ds} = 0.01 V.

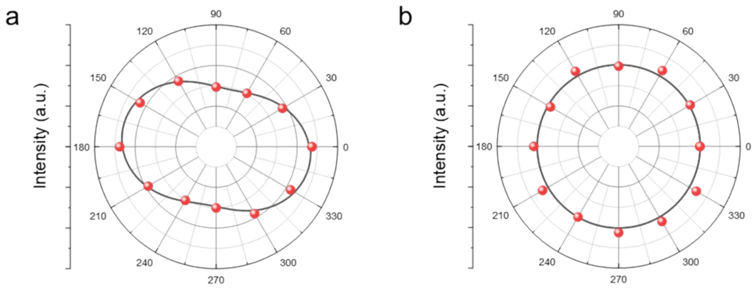

Fig. S16. The angle-resolved PL measurements of a) ZrS_3 and b) oxidized ZrS_3. Polar plot of the relationship between the laser polarization angle and the intensity of the PL peak centered at ~1.96 eV.